Pergamon

0301-9322(94)E0010-G

Int. J. Multiphase Flow Vol. 20, No. 4, pp. 775–787, 1994

0301-9322/94 $7.00 + 0.00

AN EXPERIMENTAL STUDY OF THE MENISCUS SHAPE ASSOCIATED WITH MOVING LIQUID–FLUID CONTACT LINES

A. J. J. VAN DER ZANDEN† and A. K. CHESTERS

Laboratory of Fluid Dynamics and Heat Transfer, Eindhoven University of Technology, P.O. Box 513, Eindhoven, The Netherlands

(Received 9 June 1992; in revised form 2 February 1994)

Abstract—Using a new technique involving light reflection, the interfacial curvature of a meniscus formed by a well wetting liquid steadily displacing a gas in a glass capillary has been measured down to about 50 nm from the solid. Within the domain explored, the measured meniscus curvature increases strongly as the wall is approached, in agreement with classical models which make use of the continuum approximation, no slip, etc. The inner length scale, at which such models fail, is inferred from the measurements to be of the order of a molecular dimension, suggesting that non-continuum effects dominate. A comparison of measured dynamic contact angles of liquid–liquid pairs of large viscosity ratio with a model developed earlier by the authors, incorporating such an inner length scale, suggests that the true contact angle in the advancing fluid increases significantly with line speed in one of the cases.

Key Words: wetting, dewetting, dynamic contact line

1. INTRODUCTION

It has long been known that the shape of a moving meniscus inside a tube depends on its velocity (Rose & Heins 1962). With the exception of the observations of Hansen & Toong (1971), the meniscus has been reported to be spherical, for instance by Hoffman (1975) in the case of an advancing meniscus (liquid displacing a gas) and by Fermigier & Jenffer (1988) in the liquid–liquid case. The dynamic contact angle, φ_d, between the meniscus and the wall then determines the meniscus shape.

Theoretical considerations suggest that very close to the wall a significant deviation from the spherical must occur as a result of viscous stresses and that this deviation is at least in part responsible for the observed dependence of the dynamic contact angle on the line speed [see for example Dussan V. (1979) and de Gennes (1985) for relatively recent reviews]. Indeed, were the classical approximations of no slip, of an interfacial tension and of the continuum description to apply at all distances from the line, this deviation would be indefinitely large at all non-zero line speeds.

In reality, at least the continuum approximation must lose its validity at distances from the solid of the order of a molecular dimension, thereby removing the singularity and limiting the extent of the deviation. In addition, significant slip may occur, as supposed by many authors (Dussan V. 1976; Huh & Mason 1977; Cox 1986) and as suggested by simple molecular-dynamics simulation (Thompson & Robbins 1989), while the approximation of an interfacial tension, confined to an indefinitely thin layer, must be replaced, close to the line, by a representation of the long-range intermolecular interactions as volume forces. The latter exercise has recently been carried out for a system exhibiting a small but non-zero contact angle, taking account of van der Waals interactions (de Gennes *et al.* 1990). Furthermore, in addition to the above effects, a deviation of the true contact angle from its static value may occur, associated, for example, with the adsorption and desorption processes involved in the displacement of the contact line.

†Present address: Laboratory of Separation Technology, Eindhoven University of Technology, P.O. Box 513, Eindhoven, The Netherlands.

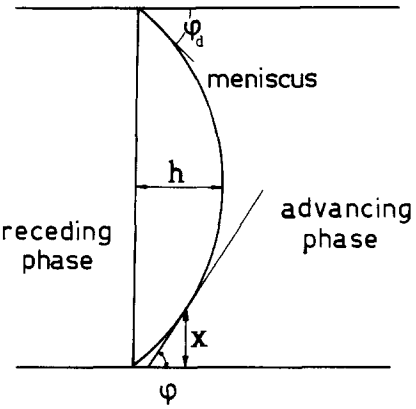

Figure 1. Definition of variables.

From the foregoing it is evident that observations of the meniscus shape close to the contact line in specific cases would be extremely helpful in sorting out the occurrence and relative importance of the various effects. Since, however, the thickness of the region adjoining a moving contact line in which the meniscus is significantly deformed is too small for this deformation to be verified visually this requires special techniques.

Using a microscope, the first part of the wall region was observed by Dussan V. *et al.* (1991), at a distance of between 3×10^{-4} and 2×10^{-5} m from the wall, for an advancing meniscus formed by immersing a glass cylinder in silicone oil.

At molecular distances from the wall the shape of a liquid–gas interface of a spreading drop has been measured via ellipsometry by Heslot *et al.* (1989a, b, c, 1990). These experiments showed clearly a "step-like" shape very close to the contact line which was supposed to be a result of the layering of the molecules.

In the present study two groups of experiments are described. The first involves a new technique, developed to measure the curvature of an advancing liquid–gas meniscus in a capillary tube sufficiently close to the wall to cover a large part of the deformed region. The second group concerns observations of the dynamic contact angle in both advancing and receding cases. To arrive at fluids exhibiting non-zero static contact angle (φ_s) on glass, liquid–liquid rather than liquid–gas systems were chosen, using a large viscosity ratio to minimize the role of viscous forces in the less viscous phase. These results considerably extend the range of viscosity ratios examined to date.

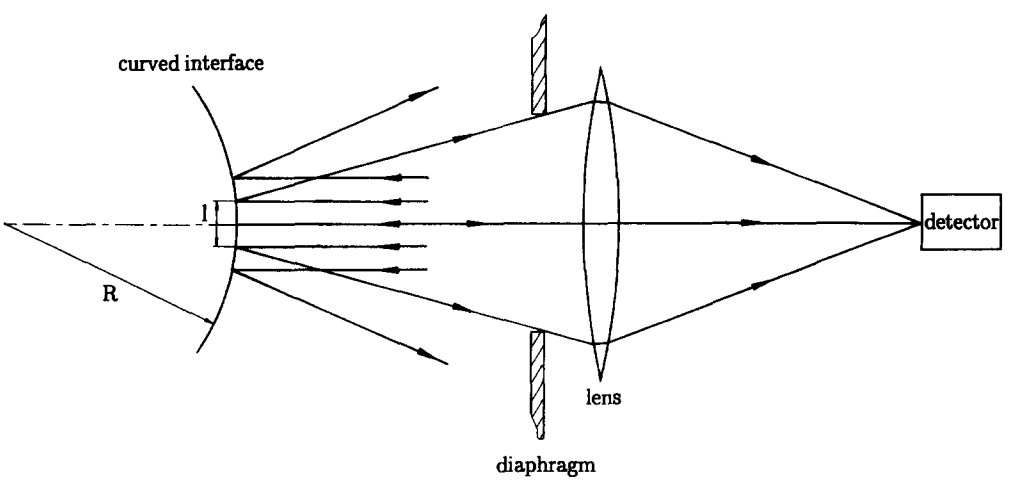

Figure 2. The basis of the measuring technique used for measuring the curvature of a (partially) reflecting curved interface.

The results obtained are examined with interest in the following questions:

(a) Does the meniscus curvature increase strongly as the wall is approached?
(b) If so, down to what distance (inner length scale, λ) from the wall does this strong increase continue?
(c) Does the meniscus shape correspond quantitatively with any existing model?
(d) Is the true contact angle, φ_0, a function of line speed?

These questions are, in fact, related since all models incorporate some deviation from classical behaviour which effectively defines the inner length scale (slip length, molecular dimension, etc.) and require some assumption regarding the true contact angle. The four questions thus effectively reduce to a single question (c).

Most of the available models are not applicable to the present measurements, being either confined to the limit of vanishingly small line speeds or concerning finite-element simulations of specific situations. These limitations do not apply to an approximate model developed earlier by the authors (section 2). Though incorporating an inner boundary condition reflecting breakdown of the continuum description, the model agrees excellently with finite-element simulations (based on breakdown of the no-slip condition) at distances from the wall considerably greater than λ (the "outer" region). It is noteworthy that in this region, which certainly includes that involved in the measurement of the dynamic contact angles, all models appear to be equivalent for appropriate choices of λ and φ_0. Hence, while data on dynamic contact angles provide the first indication of the order of magnitude of λ and of any line-speed dependence of φ_0, they provide no information on the appropriate model of the inner region. Data on the meniscus shape close to the wall should enable much harder conclusions to be drawn regarding these parameters and possibly permit a choice between models (i.e. between inner boundary conditions).

A brief description of the approximate model and its correspondence with existing observations is presented in the next section. Measurements of meniscus curvature and dynamic contact angle are presented in sections 3 and 4, respectively, accompanied by the corresponding predictions of the model. These results are discussed in section 5, with interest both in the implied values of λ and φ_0 and in the underlying mechanisms.

2. THE MODEL OF THE MENISCUS SHAPE

An approximate model for the shape of a steadily moving meniscus in a tube has been developed by the present authors in a series of articles (henceforth referred to as papers I, II and III), beginning with the liquid–gas advancing and receding cases (Boender *et al.* 1991; Chesters & van

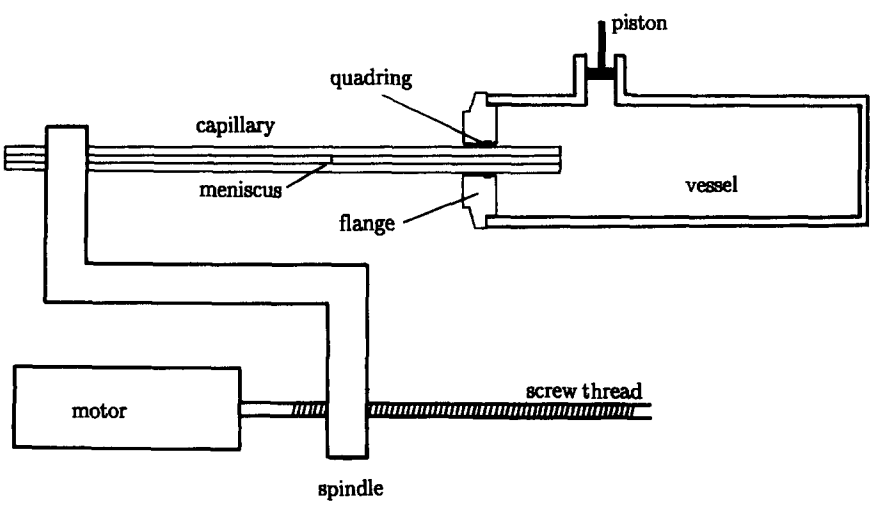

Figure 3. Experimental set-up to measure meniscus curvatures.

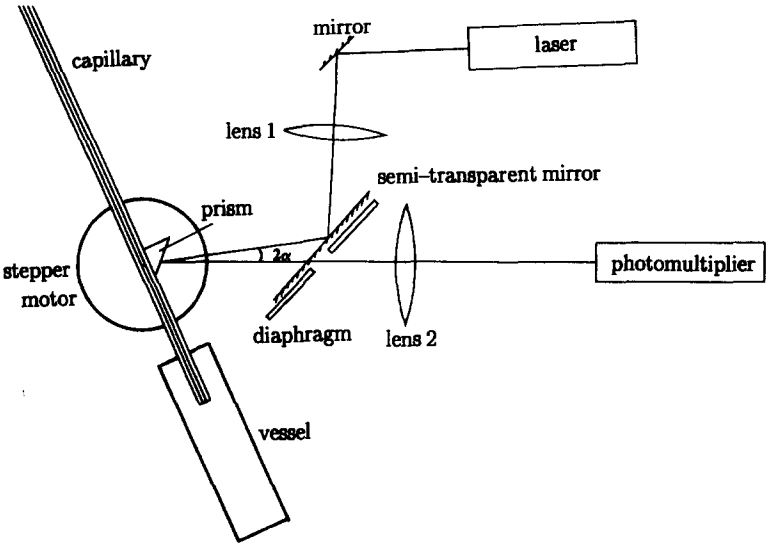

Figure 4. Overall set-up for measuring the curvature of a meniscus in the wall region.

der Zanden 1993) and extending the model to the liquid–liquid case (van der Zanden & Chesters 1994) (see also van der Zanden 1993). The model, based on the classical description of the fluids down to a distance λ from the wall, results in a second-order ordinary differential equation for the meniscus inclination, φ, as a function of distance, x, from the wall (figure 1):

$$\frac{\mathrm{d}}{\mathrm{d}x}\left(\sin\varphi\frac{\mathrm{d}\varphi}{\mathrm{d}x}+\frac{\cos\varphi}{a-x}\right)=\frac{2\sin\varphi}{x^2}\mathrm{Ca}\left(\frac{\mu_\mathrm{R}}{\mu_\mathrm{A}}c_\mathrm{R}\sin\varphi+\frac{\mu_\mathrm{R}}{\mu_\mathrm{A}}d_\mathrm{R}\cos\varphi-c_\mathrm{A}\sin\varphi-d_\mathrm{A}\cos\varphi\right), \quad [1]$$

with μ_A and μ_R the dynamic viscosity of the advancing and receding liquid, respectively, and c_R, c_A, d_R and d_A as given in appendix A. a is the tube radius. The capillary number, Ca, is the line speed U in the advancing phase made dimensionless with μ_A and the interfacial tension σ

$$\mathrm{Ca}=\frac{\mu_\mathrm{A}U}{\sigma}. \quad [2]$$

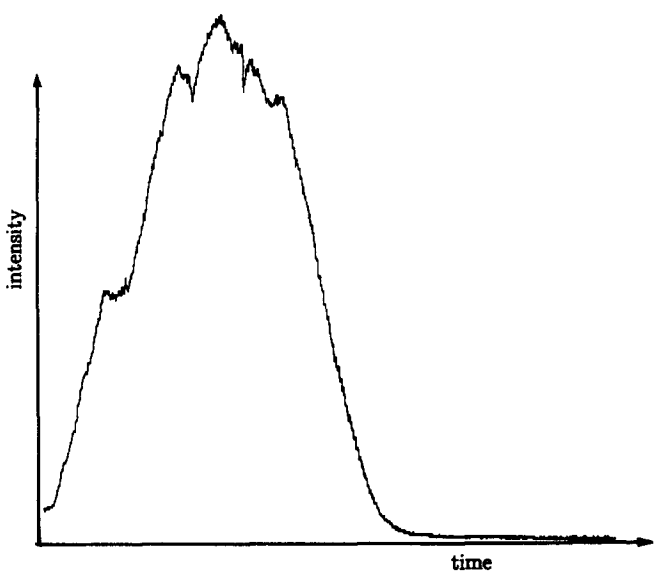

Figure 5. Intensity record of the reflected light during the passage of a meniscus through the laser beam.

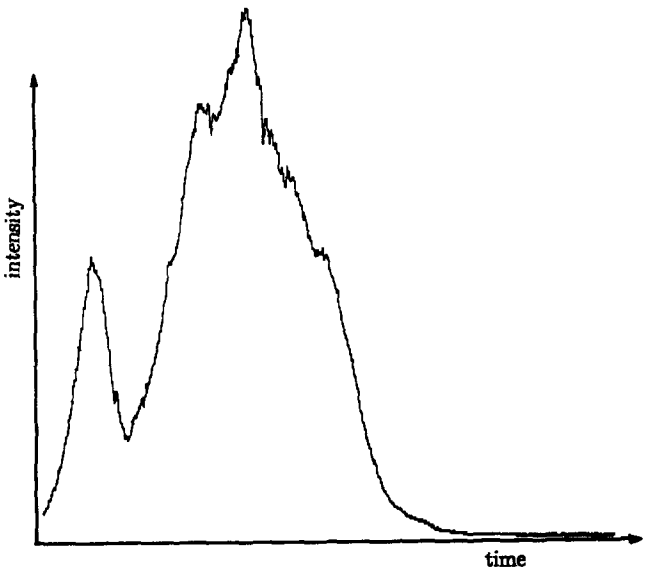

Figure 6. More ragged intensity record of the reflected light during the passage of a meniscus through the laser beam.

The applied inner boundary condition is that of specified φ at distance λ from the wall. Agreement was obtained between prediction and available measurements of dynamic constant angle if λ was taken to be of the order of a molecular dimension and the corresponding value of φ_0 was therefore termed the true contact angle, since it could be interpreted as the final meniscus inclination.

In the advancing case the predicted meniscus shape proved relatively insensitive to the values of both λ and φ_0 and good agreement with experimental data on φ_d was obtained taking $\lambda = 10^{-9}$ m (of the order of a molecular dimension) and $\varphi_0 = \varphi_s$ (paper I). In the receding case, in which a film of liquid is left behind on the wall above some critical capillary number, the predicted meniscus shape is sensitive to the value of φ_0 and evidence for significant deviation of φ_0 from φ_s at the critical capillary number was found (paper II). In the liquid–liquid case, in which one of the liquids is always receding, and the meniscus shape is again sensitive to the value of φ_0, evidence was once more found for a departure of φ_0 from φ_s in certain systems (paper III).

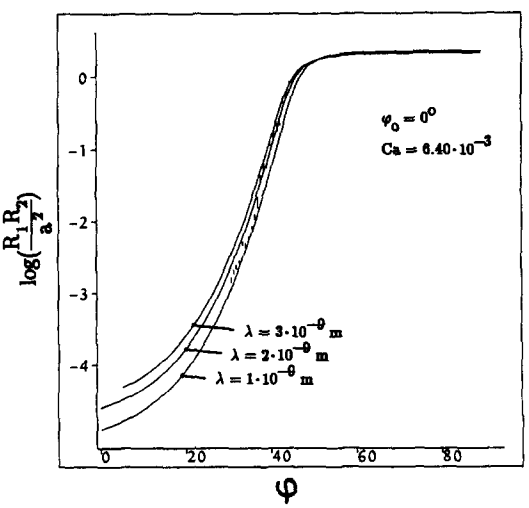

Figure 7. Comparison of the experimental results (error bars) with the prediction of the model for three λ-values (continuous lines), for given Ca and varying φ.

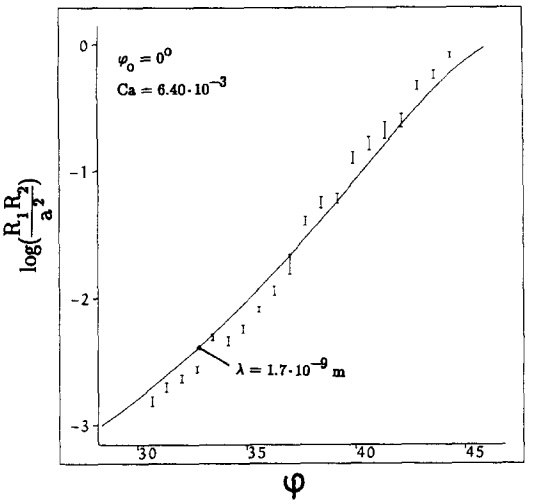

Figure 8. Comparison of the experimental results (error bars) with the best fit of the prediction of the model ($\lambda = 1.7 \times 10^{-9}$ m), for given Ca and varying φ.

The dynamic, or apparent, contact angle, φ_d, is defined here as

$$\varphi_d = \cos^{-1}\left(\frac{2ha}{a^2 + h^2}\right) \qquad [3]$$

where h is the apex height of the meniscus (figure 1). For a spherical meniscus φ_d equals the contact angle at the wall.

3. DETERMINATION OF THE MENISCUS CURVATURE IN THE VICINITY OF AN ADVANCING LIQUID–GAS CONTACT LINE

Experimental set-up

The basic principle of the measurement is illustrated in figure 2. A parallel laser beam uniformly illuminates a portion of the interface and by use of a diaphragm the intensity of the light reflected within a small angle of the incident direction is measured. Since the interface is unequally curved in the two principal directions, the light received originates from an elliptical portion of the interface with major and minor axes, l_1 and l_2, proportional to the principal radii of curvature R_1 and R_2†. Neglecting wave effects, the detected intensity is proportional to the area of the ellipse and hence to the product $R_1 R_2$. The region of the interface examined is simply that normal to the chosen laser direction.

The application of the principle of figure 2 to an advancing meniscus in a capillary tube is depicted in figure 3. A glass capillary with external diameter 6.0 mm and internal diameter 1.7 mm is partially filled with liquid. The capillary can move in and out of a vessel which is filled with the same liquid. A movement of the capillary into the vessel, imposed by a servo motor, causes the liquid–gas meniscus in the capillary to advance in the opposite direction.

The capillary tube is fastened on a stepper motor (figure 4). An almost parallel laser beam illuminates a small portion of the meniscus, lens 1 determining the size of the illuminated spot. The spot size must not be too small as the measuring technique is based on the assumption that the portion of the meniscus from which the reflected intensity is measured is uniformly illuminated. The prism mounted against the capillary permits the required range of angles of incidence. Between the prism and the capillary a drop of decalin (refractive index equal to that of the glass) prevents refraction at the outer tube wall. The angle between the laser beam impinging on the meniscus and the reflected rays through the diaphragm was not zero but approx. 5° ($=2\alpha$: figure 4). This was

†Note that this implicitly assumes the angle of collection to be constant. Since the reflected light originates from a virtual source a distance $R/2$ behind the interface and since R is in reality much smaller than the distance between interface and diaphragm, this is justified.

done to avoid scattered light from the laser beam incident on the semi-transparent mirror entering the photomultiplier. A small mirror, instead of the semi-transparent mirror, could also have been used. The stepper motor in figure 4 can rotate the capillary and the vessel so that measurements can be carried out for different φ-values. The angle of the laser beam in the liquid is calculated from Snell's law. The corresponding value of φ is obtained allowing for the fact that the laser is not quite normal to the reflecting region of the meniscus but inclined at a small angle, α.

Measuring procedure

To insure cleanliness, the capillary and the inside of the vessel were first washed with chromic acid. Afterwards both were rinsed with distilled water and dried in an oven for about half an hour at round 120°C. The vessel was filled with silicon oil of moderately high viscosity ($\mu = 0.552\,\mathrm{kg\,m^{-1}\,s^{-1}}$, $\sigma = 2.22 \times 10^{-2}\,\mathrm{N\,m^{-1}}$, static contact angle 0°). The use of a much higher viscosity would have required very small velocities for a given capillary number. Temperature fluctuations of the liquid in the vessel would then superimpose a comparable additional velocity. The use of a much smaller viscosity could have led to inertial effects, which are not included in the theoretical model.

The moving meniscus traverses the laser beam and the intensity of reflected light is measured. The intensity detected by the photomultiplier shows a peak as the meniscus passes the laser beam (figure 5). At the moment the maximum intensity, I_{max}, is registered, the meniscus is in the centre of the laser beam. As was argued before, I_{max} is proportional to the product of the principal radii of curvature. To obtain this product, the system was calibrated for each angle of incidence using known radii of curvature. For this purpose a very slowly receding meniscus was used. Although a thin film is left behind, the (equal) radii of curvature of a slowly receding meniscus are very nearly equal to that of the capillary, a. Note that this calibration also eliminates the effect of unequal weighting of the contributions from R_1 and R_2, caused by refraction at the inner tube wall and outer prism surface (resulting in unequal collecting angles of these contributions at the interface). For the same reason it is not necessary that the diaphragm be normal to the collected light.

A contact line formed by a liquid with zero static contact angle cannot recede. Thus a given region of the capillary can be used only once. To carry out further measurements, the capillary and the vessel in figure 4 can be displaced so that the laser beam shines on a dry part of the capillary. The measurement of the advancing meniscus can then be repeated followed by calibration with the slowly "receding" meniscus. After each measurement of an advancing meniscus follows a measurement of a "receding" meniscus.

To avoid stick–slip phenomena between the quadring and the capillary (figure 3), the outside of the capillary which moves into the vessel is prewetted with the silicon oil as used for the meniscus.

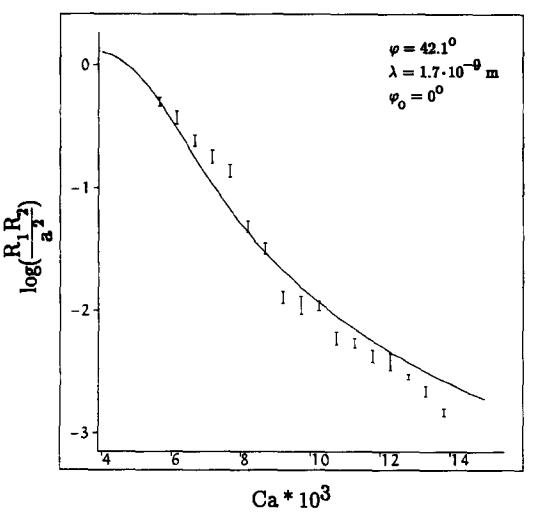

Figure 9. Comparison of the experimental results (error bars) with the prediction of the model ($\lambda = 1.7 \times 10^{-9}$ m), for given φ and varying Ca.

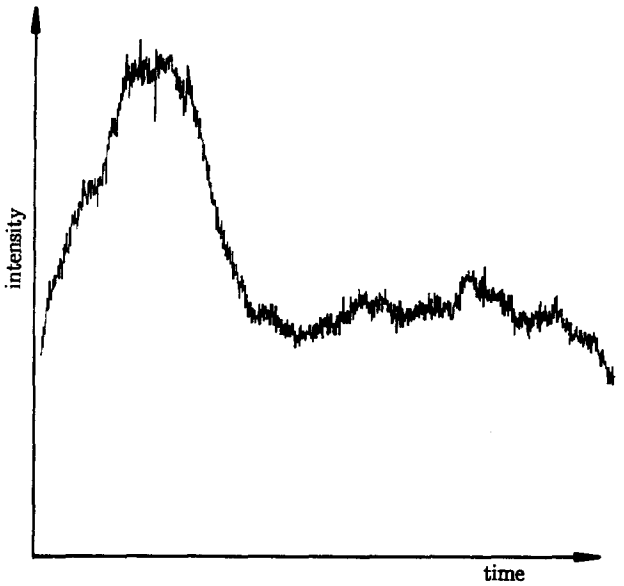

Figure 10. Intensity of the reflected light during the passage of a meniscus through the laser beam for the smallest measured radius of curvature.

This lubrication makes a smoother motion of the meniscus possible. Even then, not every record of intensity was as smooth as in figure 5. Intensities with a more "ragged" appearance, as depicted in figure 6, were also registered.

When the entire capillary has been used it is first rinsed with hexane and then with water, after which the washing procedure with chromic acid and distilled water is repeated. All measurements are performed with the same capillary over a length of approx. 20 cm.

Results

In figure 7 the results of the measurements for $Ca = 6.40 \times 10^{-3}$ are presented (the error bars), together with the predictions of the model for various λ-values, taking the true contact angle, φ_0 as constant at 0°. Every bar is the result of at least ten measurements. φ denotes the local inclination of the meniscus, varying from 90° at the tube centre to φ_0 at the wall. The term $R_1 R_2/a^2$, an inverse measure of the meniscus curvature, is constant in the central, spherical portion of the meniscus and decreases in the wall region. The best fit is obtained for a λ-value of 1.7×10^{-9} m (figure 8). A small systematic deviation remains.

Figure 9 presents complimentary measurements at a fixed value of φ for various Ca-values. The corresponding model predictions are once more based on $\lambda = 1.7 \times 10^{-9}$ m and $\varphi_0 = 0°$. A similar deviation is observed, the model overestimating the smaller values of $R_1 R_2$ and underestimating the larger.

The limit of measurable intensity was posed by the background intensity which ultimately becomes comparable with that of the reflection peak, as illustrated in figure 10. In the series presented in figure 8, the final measurement point corresponds to $x = 4.6 \times 10^{-8}$ m and $R_1 = 1.5 \times 10^{-6}$ m, where x (distance from the wall) and R_1 have been calculated with the help of

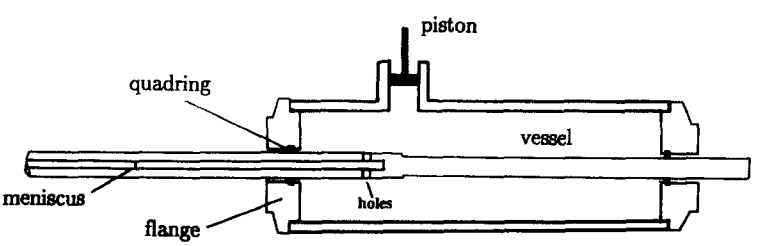

Figure 11. Experimental set-up to measure dynamic contact angles.

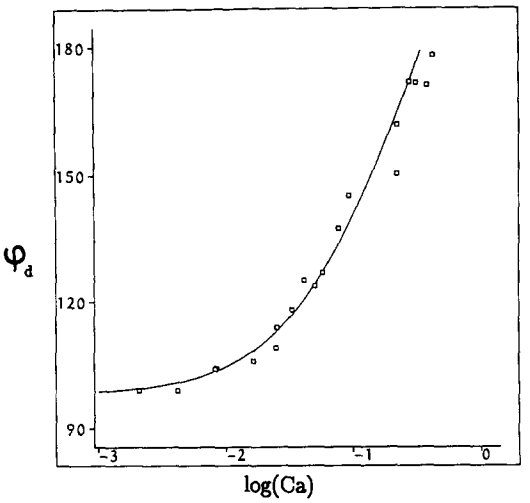

Figure 12. The Ca-dependence of φ_d for glycerine displacing hexane ($a = 8.61 \times 10^{-4}$ m).

the model. For the series in figure 9, the corresponding figures are respectively 8.3×10^{-8} and 1.7×10^{-6} m. Since these R_1-values are only a few times the wavelength of the laser light, it is likely that wave (i.e. diffraction) effects are becoming significant and the interpretation of the signal then becomes difficult anyway.

Finally, we note that an attempt was also made to apply the technique to a receding liquid–gas contact line. It did not, however, prove possible to obtain any information on the meniscus shape in the wall region since a receding meniscus with a static contact angle below 90° can have two points on the meniscus on which the laser light impinges perpendicularly: one in the outer region of the meniscus and one in the wall region. The light reflected onto the photomultiplier from the point in the wall region is drowned by that from the point in the outer region.

4. DYNAMIC CONTACT ANGLES FOR LIQUID–LIQUID COMBINATIONS OF LARGE VISCOSITY RATIO

Experiments

In order to measure dynamic contact angles of a meniscus formed by two liquids in a capillary, a set-up has been constructed as shown in figure 11. With the help of the servo motor a glass

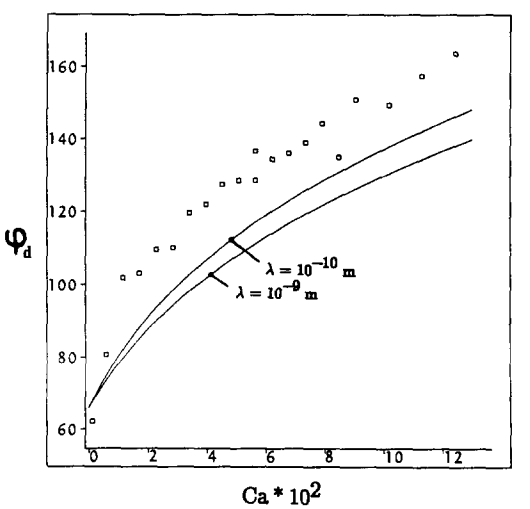

Figure 13. The Ca-dependence of φ_d for glycerine displacing a low-viscosity silicon oil ($a = 8.28 \times 10^{-4}$ m).

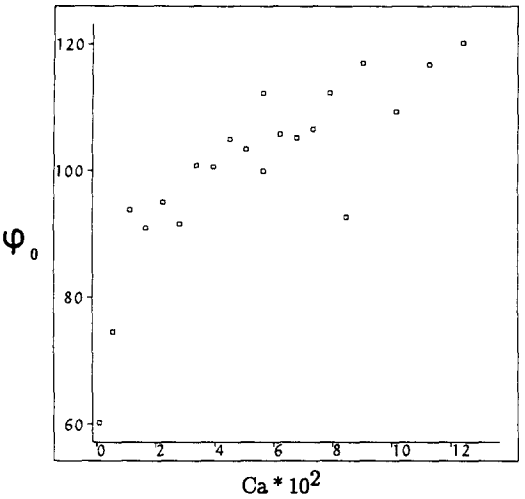

Figure 14. Variation of φ_0 with Ca required to obtain agreement between computations and experiments in the case studied in figure 13.

capillary and rod combination can be made to move through the vessel filled with liquid. The liquid in the vessel has access to the capillary via two holes in its wall. The dimensions of the capillary and the rod are chosen such as to produce a moving meniscus which moves with respect to the capillary but not with respect to the laboratory frame. The piston serves to adjust the position of the meniscus. With a computer the motor is made to move with a constant velocity. The result is that the meniscus moves through the capillary with a constant velocity. The dynamic contact angles were determined by taking photographs and measuring the apex height of the meniscus [3]. A microscope slide mounted against the capillary with decalin (having the same index of refraction as glass) in between prevented light refraction from the outer tube wall.

Results

The first liquid combination used was glycerine ($\mu = 1.47\,\mathrm{kg\,m^{-1}\,s^{-1}}$) displacing hexane ($\mu = 3.68 \times 10^{-4}\,\mathrm{kg\,m^{-1}\,s^{-1}}$, $\mu_R/\mu_A = 2.5 \times 10^{-4}$) with interfacial tension $2.52 \times 10^{-2}\,\mathrm{N\,m^{-1}}$ (measured by the Wilhelmy plate method). In figure 12 the results are compared with the model taking $\lambda = 10^{-9}\,\mathrm{m}$ and $\varphi_0 = 98°$. The agreement is good, confirming the order of magnitude of λ and implying that, in this case, the approximation of constant φ_0 is acceptable.

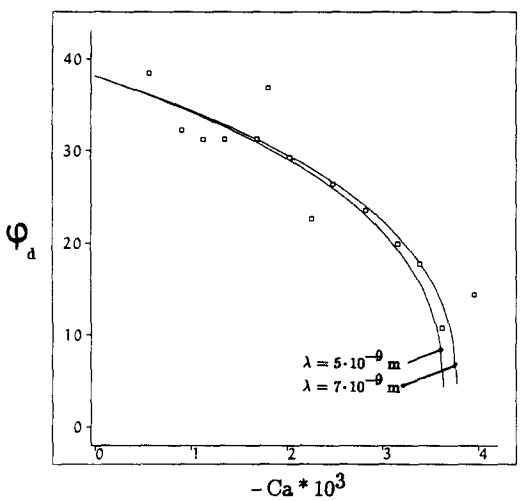

Figure 15. The Ca-dependence of φ_d in the same case as studied in figure 13. For ease of comparison with receding liquid–gas data, φ_d and Ca have been based on the more viscous phase ($\mathrm{Ca} = -\mu_R U/\sigma$).

The second liquid combination used was glycerine ($\mu = 0.995\,\mathrm{kg\,m^{-1}\,s^{-1}}$) displacing a low viscous silicon oil ($\mu = 4.79 \times 10^{-3}\,\mathrm{kg\,m^{-1}\,s^{-1}}$, $\mu_R/\mu_A = 4.81 \times 10^{-3}$) with interfacial tension $1.99 \times 10^{-2}\,\mathrm{N\,m^{-1}}$ (measured by the pendent drop method). In figure 13 the results are compared with the model taking $\varphi_0 = 66°$ and $\lambda = 10^{-9}$ or 10^{-10} m. The measurements deviate significantly from the predictions of the model. The agreement could be improved by choosing a smaller λ-value. However, in view of the size of the molecules this would be physically unacceptable. A more obvious choice which leads to better agreement is to abandon the assumption that the true contact angle remains equal to the static value. In figure 14 the true contact angle at the wall needed to obtain agreement between model ($\lambda = 10^{-9}$ m) and experiments as a function of the capillary number.

Finally the same liquid combination was used with the silicon oil as the advancing liquid and the glycerine as the receding. In figure 15 the measurements are shown to agree with the predictions of the model, taking $\varphi_0 = 38°$ and λ around 6×10^{-9} m.

5. DISCUSSION

The measurements presented in section 3 provide direct confirmation of the existence of a wall region in which the meniscus curvature increases strongly as the advancing contact line is approached. As the final measuring station is still quite far from the wall in molecular terms, it cannot be concluded that the entire difference between the dynamic and static contact angles is apparent, as the true contact angle may not be zero. A glance at the first series of measurements, however, indicates that at the last measuring station, around 50 nm from the wall, the meniscus inclination has already fallen to about 30°, while the curvature is very strong ($R_1 \sim 1\ \mu$m). Clearly, therefore, the true contact angle must be considerably smaller than 30°.

If it is supposed that the true contact angle in this case is at any rate less than 20° then the best-fit value of λ is found to be at most a factor 2 larger than the 1.7 nm obtained taking φ_0 to be zero. This leads to the important conclusion that, at least in the present case, the inner length scale which governs the behaviour in the wall region is of the order of molecular dimensions. While this conclusion was tentatively reached in papers I–III, as well as by other authors such as Lowndes (1980), the present results leave much less margin for doubt.

We note at this point that de Gennes *et al.* (1990) concluded that for very small static contact angles the inner length scale should be determined by deviations from classical behaviour associated with long-range intermolecular (van der Waals) forces. In the small-Ca limit which they treat, their equation for the meniscus shape corresponds to our own (see appendix B), the role of the length scale λ now being played by the parameter $L/(2\varphi_s^2)$, where L is the length scale $\sqrt{A/(6\pi\sigma)}$ (A = the Hamaker constant). Since A is typically of the order of 10^{-20} J, this length scale should be the dominant one for small φ_s-values, becoming greater than 10 nm for φ_s-values less than about 5°. At first sight this conclusion would appear to be in conflict with the present findings. The present case of zero φ_s is, however, excluded by their theory.

While a λ-value of the order of a nanometer provides a reasonable fit of the experimental results, a certain systematic deviation appears to remain (figures 7–9). Various possible explanations present themselves, such as:

(1) Fluid dynamic approximations incorporated in the theoretical model.
(2) Error in the inferred meniscus curvatures, due to the wave nature of light.
(3) Behaviour in the inner region complicated by multiple length scales (reflecting various deviations from classical behaviour, such as that considered by de Gennes *et al.* 1990), of which the molecular scale λ is merely the most prominent).
(4) Deviation of the true contact angle from the static value.
(5) Inhomogeneities in the solid surface.

While at present it is not possible to rule out any of these effects, (1) and (4) appear unlikely, at least as complete explanations. Predictions of the approximate model in the liquid–gas advancing case agreed with finite-element results of Lowndes (1980) within about a degree (paper I), while the hypothesis that the true contact angle increases with line speed could improve the agreement in figure 9 but not in figure 8.

Turning to possibility (2), the smallest radii of curvature involved are only a few times the wavelength of light. As noted in section 4, wave effects then almost certainly become significant. To explain the discrepancy, these effects would need to reduce reflection at higher curvatures. While such effects should be theoretically predictable, the problem appears to be a complex one, involving not only the influence of the ratio R_1/Λ on the coefficient of normal reflection but also the effect of the nearby solid surface (Λ = wavelength of light). Possibility (3)—of additional length scales—has been touched on above. Surface inhomogeneity [possibility (5)], which also introduces new length scales, is discussed below in the context of the dynamic-angle measurements.

The measurements presented in section 4 extend those of Fermigier & Jenffer (1988), discussed in paper III, in which the largest value of μ_R/μ_A was 0.9 (as compared with around 200 in the present study) and the smallest 7.6×10^{-3} (as compared with 2.5×10^{-4} here). The comparison of the new data with predictions of the model provides the same picture, however, in some cases the behaviour is adequately predicted taking $\varphi_0 = \varphi_s$, in others a significant increase in φ_0 (measured in the advancing phase) with Ca must be supposed in order to obtain agreement.

The simplest explanation of the line-speed dependence of φ_0 in some cases is that this reflects variation in the true advancing angle, associated with the kinetics of desorption of the receding fluid and adsorption of the advancing. Intuitively it is credible that desorption may be rate-limiting for a liquid but not for a gas and this accords with data in advancing liquid–gas cases, which have so far been well described by a constant φ_0-value. Likewise large molecules of silicon oil might be expected to desorb more slowly than those of hexane (figures 13 and 12, respectively). The fact that the advancing mode of the glycerine–silicon system exhibits a deviation of φ_0 from φ_s, while the receding mode does not, should not be considered significant; the largest Ca-values in the receding case are less than those at which significant deviation is observable in the advancing case.

It should be noted however that the results for the same pair of liquids in both the advancing and the receding modes indicate that considerable hysteresis (28°) exists in the static contact angle. The presence of hysteresis points to non-ideality of the wall (roughness/chemical heterogeneity). The relationship between the dynamic contact angle and the capillary number must be influenced by this heterogeneity, which will modify the fluid motion on the scale concerned. It is conceivable that such effects appear as apparent linespeed dependence of the φ_0-value and that this, rather than variation of the true contact angle, is involved. It seems likely that such uncertainty will remain until reliable models of the effects of surface heterogeneity, which is virtually always present in reality, have been developed.

REFERENCES

BOENDER, W., CHESTERS A. K. & VAN DER ZANDEN A. J. J. 1991 An approximate analytical solution of the hydrodynamic problem associated with an advancing liquid–gas contact line. *Int. J. Multiphase Flow* **17,** 661–676.

CHESTERS, A. K. & VAN DER ZANDEN, A. J. J. 1993 An approximate solution of the hydrodynamic problem associated with receding liquid–gas contact lines. *Int. J. Multiphase Flow* **19,** 905–912.

COX, R. G. 1986 The dynamics of the spreading of liquids on a solid surface. Part 1. Viscous flow. *J. Fluid Mech.* **168,** 169–194.

DUSSAN V., E. B. 1976 The moving contact line: the slip boundary condition. *J. Fluid Mech.* **77,** 665–684.

DUSSAN V., E. B. 1979 On the spreading of liquids on solid surfaces: static and dynamic contact lines. *A. Rev. Fluid Mech.* **11,** 371–400.

DUSSAN V., E. B., RAMÉ, E. & GAROFF, S. 1991 On identifying the appropriate boundary conditions at a moving contact line: an experimental investigation. *J. Fluid Mech.* **230,** 97–116.

FERMIGIER, M. & JENFFER, P. 1988 Dynamics of a liquid–liquid interface in a capillary. *Ann. Phys.* **13,** 37–42.

DE GENNES, P. G. 1985 Wetting: statics and dynamics. *Rev. Mod. Phys.* **57,** 827–863.

DE GENNES, P. G., HUA, X. & LEVINSON, P. 1990 Dynamics of wetting: local contact angles. *J. Fluid Mech.* **212,** 55–63.

HANSEN, R. J. & TOONG, T. Y. 1971 Interface behavior as one fluid completely displaces another from a small diameter tube. *J. Colloid Interface Sci.* **36,** 410–413.

HESLOT, F., CAZABAT, A. M. & FRAYSSE, N. 1989a Diffusion-controlled wetting films. *J. Phys.: Condens. Matter* **1,** 5793–5798.

HESLOT, F., FRAYSSE, N. & CAZABAT, A. M. 1989b Molecular layering in the spreading of wetting liquid drops. *Nature* **338,** 640–642.

HESLOT, F., CAZABAT, A. M. & LEVINSON, P. 1989c Dynamics of wetting of tiny drops: ellipsometric study of the late stages of spreading. *Phys. Rev. Lett.* **62,** 1286–1289.

HESLOT, F., CAZABAT, A. M., LEVINSON, P. & FRAYSSE, N. 1990 Experiments on wetting on the scale of nanometers: influence of the surface energy. *Phys. Rev. Lett.* **65,** 599–602.

HOFFMAN, R. L. 1975 A study of the advancing interface I. Interface shape in liquid–gas systems. *J. Colloid Interface Sci.* **50,** 228–241.

HUH, C. & MASON, G. 1977 The steady movement of a liquid meniscus in a capillary tube. *J. Fluid Mech.* **81,** 401–419.

LOWNDES, J. 1980 The numerical simulation of the steady movement of a fluid meniscus in a capillary tube. *J. Fluid Mech.* **101,** 631–646.

ROSE, W. & HEINS, R. W. 1962 Moving interfaces and contact angle rate-dependency. *J. Colloid Sci.* **17,** 39–48.

THOMPSON, P. A. & ROBBINS, M. O. 1989 Simulations of contact-line motion: slip and the dynamic contact angle. *Phys. Rev. Lett.* **63,** 766–769.

VAN DER ZANDEN, A. J. J. 1993 The hydrodynamics of a moving fluid liquid contact line. Ph.D. thesis, Eindhoven University of Technology, Eindhoven, The Netherlands.

VAN DER ZANDEN, A. J. J. & CHESTERS, A. K. 1994 An approximate solution of the hydrodynamic problem associated with moving liquid–liquid contact lines. *Int. J. Multiphase Flow* **20,** 789–798.

APPENDIX A

The coefficients $c_R \ldots d_A$ are:

$$c_R = S^2[S^2 - \delta\varphi + R(\varphi^2 - S^2)]/D, \qquad [A1]$$

$$d_R = SC[S^2 - \delta\varphi + R(\varphi^2 - S^2) - \pi \tan \varphi]/D, \qquad [A2]$$

$$c_A = S^2[S^2 - \delta^2 + R(\delta\varphi - S^2)]/D, \qquad [A3]$$

$$d_A = SC[S^2 - \delta^2 + R(\varphi\delta - S^2) - R\pi \tan \varphi]/D, \qquad [A4]$$

where $S \equiv \sin \varphi$, $C \equiv \cos \varphi$, $\delta \equiv \varphi - \pi$, $R \equiv \mu_R/\mu_A$ and

$$D \equiv (SC - \varphi)(\delta^2 - S^2) + R(\delta - SC)(\varphi^2 - S^2). \qquad [A5]$$

APPENDIX B

Taking account of van der Waals forces, de Gennes *et al.* derived an expression for the meniscus shape in the region where the classical hydrodynamic approximations apply, for the limiting case of small values of the parameters φ_s and $3\,\mathrm{Ca}/\varphi_s^3$:

$$\varphi = \varphi_s\left[1 + \frac{3\mathrm{Ca}}{\varphi_s^3}\ln\left(\frac{x}{\lambda}\right)\right], \qquad [B1]$$

where

$$\lambda = \frac{\sqrt{A}}{2\varphi_s^2\sqrt{(6\pi\sigma)}}. \qquad [B2]$$

Making use of the fact that $3\,\mathrm{Ca}/\varphi_s^2 \ll 1$, this equation can be written

$$\varphi^3 = \varphi_s^3 + 9\,\mathrm{Ca}\ln\left(\frac{x}{\lambda}\right). \qquad [B3]$$

This is the same as the small-φ_s, small-Ca limit of our own model, the length scale λ now being determined by van der Waals forces rather than by a molecular dimension.